

Spatial distribution of Far infrared emission in spiral galaxies II. Heating sources and gas-to-dust ratio

Y.D. Mayya^{1,2} and T.N. Rengarajan¹

¹*Tata Institute of Fundamental Research, Homi Bhabha Road, Mumbai 400 005, India*

²*Instituto Nacional de Astrofisica Optica y Electronica, Apdo Postal 51 y 216, 72000 Puebla, Pue., MÉXICO*
Electronic Mail: ydm@inaoep.mx and renga@tifrvax.tifr.res.in

Accepted — June 1997. To appear in Astronomical Journal, September 1997

ABSTRACT

We study the radial distribution of the temperature of the warm dust and gas-to-dust mass ratios in a sample of 22 spiral galaxies. The heating capabilities of the diffuse interstellar radiation field (ISRF), based on Désert et al. model, are investigated in 13 of the sample galaxies. In general, the temperature of the warm dust decreases away from the center, reaches a minimum value at the mid-disk and increases again in the outer parts of galaxies. Heating a mixture of small and big grains by the ISRF is able to explain the observed behavior qualitatively. However, ultraviolet photons from recent star formation events are necessary for a detailed matching of the warm dust temperature profiles. Very small grains contribute typically more than 50% to the observed flux at $60\mu\text{m}$ beyond half the disk radius in galaxies. Optical depth (τ_{60}) profiles, derived from the observed $60\mu\text{m}$ and warm dust temperature profiles, peak at or close to the galactic center. In 13 of the galaxies, where dust temperature profiles are modeled, we obtain optical depth and dust mass profiles after correction for the contaminating effects of very small grains. These profiles are combined with the gas density profiles in the literature, to generate profiles of the gas-to-dust mass ratio. The resulting gas-to-dust mass ratio decreases by a factor of 8 from the center to the optical isophotal radius, where the value approaches the local galactic value. With the understanding that the dust mass is proportional to metallicity, and that the metallicity increases towards the center of galaxies, one expects the gas-to-dust ratio to decrease towards the center, contrary to what is observed. We demonstrate that the observed steep gradient is a result of the over-estimation of the molecular mass, and can be flattened out to within a factor of 2, if the molecular hydrogen mass is recomputed assuming a metallicity dependent conversion factor from CO intensity to H_2 column density. The flattened radial profiles indicate a global gas-to-dust ratio of around 300, which is within a factor of two of the local galactic value.

Subject headings: dust – extinction – infrared radiation – heating sources – gas-to-dust ratio

1. Introduction

Infrared Astronomical Satellite (IRAS) observations have made a significant impact on our understanding of the dust content in galaxies. These observations were mainly sensitive to dust with temperature in the range 25–50 K, generally referred to as warm dust. There have been considerable debates on the heating sources of dust (Helou et al. 1985; Rengarajan & Verma 1986; Devereux et al. 1994; Walterbos & Schwering 1987; Xu & Helou 1996; Walterbos & Greenawalt 1996) and the mass contained in the cooler dust (Devereux & Young 1990; Chini & Krügel 1993). The ultraviolet (UV) photons from young hot stars are efficient in heating the dust and hence the most luminous far infrared (FIR) galaxies are inferred to be in a starburst mode. Such galaxies are characterized by high ratio of FIR to blue band luminosity. The heating provided by the non-ionizing photons from young and old stars may play an important role in regions of low levels of current star formation activity, as characterized by the low values of FIR to blue band luminosity. Investigating the heating power of the non-ionizing photons in these low-luminosity galaxies is one of the main goals of this study. From studies carried out in M31, Devereux et al. (1994) find that about 30% of the FIR luminosity comes from regions away from current star formation, whereas Walterbos & Schwering (1987) and more recently Xu & Helou (1996) and Walterbos & Greenawalt (1996) infer even higher levels of heating provided by the old disk and bulge stars.

Dust and gas in the interstellar medium (ISM) are believed to be well mixed, with a gas-to-dust mass ratio of around 160 in the local galactic surroundings (Sodroski et al. 1994). Based on global data of galaxies, Devereux & Young (1990) derive a value as high as 1000 for the gas-to-dust mass ratio in external galaxies. Considering that the IRAS observations are insensitive to the emission from dust below 25 K, the inferred high gas-to-dust ratio could be the result

of vast amounts of dust mass in cooler dust. However observations carried out at longer wavelengths to trace the cool dust have given inconclusive results regarding the amount of dust in the cool component (see Chini & Krügel 1993). Andreani et al. (1995) used millimeter (mm) continuum observations to infer emission from cool dust, and found gas-to-dust mass ratio to lie in the range 100–1000 with a mean value around 230, which is close to the local galactic value.

In a companion paper (Mayya & Rengarajan 1997; Paper I), we have studied the spatial distribution of FIR and 20 cm radio continuum (RC) emission in a sample of 22 galaxies. The galaxies were chosen with a view to study the spatial variation of warm dust temperature as well as the gas-to-dust ratio within the galaxies. In this paper, we combine the FIR data with the published gas density profiles for all the galaxies and optical data for a subsample of 13 galaxies, and address the issues of dust heating and gas-to-dust ratios in galaxies. Sec. 2 deals with the data and the analysis procedure that we have followed. Observed gradients in the warm dust temperature are compared with the dust heating models in Sec. 3. In Sec. 4, we discuss the gradients in FIR optical depth and the gas-to-dust ratios in galaxies. Concluding remarks are made in Sec. 5.

2. The sample, data and analysis procedure

Galaxies for study here, as well as in Paper I, were selected based on the following criteria. (1) The availability of 20 cm radio continuum images at 1' resolution, (2) the availability of HI and H₂ radial surface density profiles, (3) the optical angular diameter > 5' and (4) the 60 μ m flux density > 5 Jy. The last two criteria together ensure that there are significant number of resolution elements in each image, and that the galaxies are bright enough in the IRAS bands to get reliable High Resolution (HiRes) images. Among the 22 galaxies studied in Paper I, NGC 4656

does not have published radial profiles of HI and H₂ surface densities, and is replaced by NGC 4258 in the present work.

The basic properties of the sample galaxies are given in Table 1. The galaxy type, the optical diameter in arcmin at 25 B mag arcsec⁻², the axis ratio b/a and the position angle (PA) of the major axis are taken from the *Third reference catalogue of bright galaxies* (de Vaucouleurs et al. 1991; RC3 henceforth). Distances are taken from the Nearby Galaxy Catalog (Tully 1988), where a Hubble constant of 75 km s⁻¹ Mpc⁻¹ is assumed. The total (1–1000 μ m) FIR luminosity (L_{fir}) to optical blue band luminosity (L_{B}) ratio is calculated using the formula,

$$\frac{L_{\text{fir}}}{L_{\text{B}}} = \frac{1.26 \times 10^{-11} C (2.58 S_{60} + S_{100})}{5.98 \times 10^{-6} 10^{-0.4 B_{\text{T}}^0}}, \quad (1)$$

where C corrects for the flux outside the 60 and 100 μ m bands and is tabulated by Helou et al. (1988) as a function of temperature for a single temperature model. For the observed range of dust temperatures in galaxies, C lies between 1.3–2.0 with a typical value of 1.5. L_{B} is the true in-band B luminosity. We note that Young et al. (1989) transformed magnitude B_{T}^0 to fluxes using the absolute B magnitude of the Sun and hence their formula results in the over-estimation of L_{B} and hence the under-estimation of the ratio $L_{\text{fir}}/L_{\text{B}}$ by a factor $L_{\odot}/L_{\text{B}\odot} = 9$. S_{60} and S_{100} are the global 60 μ m and 100 μ m flux densities (in units of Jy) respectively. The denominator and numerator are in units of erg cm⁻² s⁻¹. The sources of HI and H₂ data appear in the last two columns of Table 1 respectively. Note that the H₂ data is unavailable for NGC 3198. For galaxies with known metallicity gradients (Zaritsky et al. 1994), the oxygen abundance at 3 kpc and its gradient in dex/kpc are given. Thirteen of the galaxies have archival CCD data available at broad optical bands, based on observations at the Palomar Observatory (Frei et al. 1996). These CCD images are ideal in the investigation of dust heating by the non-ionizing photons.

We use the HiRes images (Rice 1993) of the galaxies at the four IRAS bands in this work. The HiRes resolutions at 60 μ m in arcsec along two perpendicular directions are given in Table 1. The resolution is better at 12 and 25 μ m bands, but the sensitivities in these bands are too poor to trace out the outer regions in most of the galaxies in our sample and hence these images have only limited use in this study. The HiRes processing was done under the default configuration, which results in frames of 1° × 1° field with 15'' pixels. Sub-images of 60 × 60 pixels are extracted for all galaxies except NGC 2403 and 4258, for which sections of size 100 × 100 pixels are extracted. In all cases, images from the 20th iteration are used. Contour diagrams of program galaxies at 60 μ m are presented in Paper I.

Surface brightness profiles of HiRes images are obtained by azimuthally averaging over elliptical annuli of 1' width. The ellipticity and position angle of the annuli are fixed at their optical value as tabulated in Table 1. These radial profiles are used to obtain the S_{60} to S_{100} color profile, which is transformed into a dust temperature profile using the λ^{-1} emissivity law and the Planck's function. We refer to the resultant profiles as warm dust profiles. The physical temperature of the dust in any region in a galaxy depends on the type and size distribution of dust particles, effective wavelength of the heating source and the distance of the heating source from the dust particles. As all these quantities can vary within a single annulus, the derived warm dust temperature is expected to match the local dust temperature only if there is a single type of grain. In reality, the ISM contains a mixture of different grain types, and hence, the derived warm dust temperature is a flux-weighted mean of all the grain temperatures.

The optical depth of the FIR emitting dust at 60 μ m (τ_{60}) is defined by the equation,

$$\tau_{60} = \frac{S_{60}}{B(60, T_{\text{d}})}, \quad (2)$$

for the optically thin case ($\tau_{60} \ll 1$). S_{60} and $B(60, T_d)$ in the above equation are respectively the observed intensity within the $60\mu\text{m}$ band and the Planck function at the estimated temperature T_d and wavelength $60\mu\text{m}$. Observed warm dust temperature profiles and the $60\mu\text{m}$ surface brightness profiles are used in obtaining τ_{60} profiles. τ_{60} is transformed into a dust mass surface density Σ_d using the formula

$$\Sigma_d(\text{M}_{\odot}\text{pc}^{-2}) = 108\tau_{60}, \quad (3)$$

where the constant 108 is a measure of the dust size distribution and the scattering properties of the dust, and is computed based on the constants in Hildebrand (1983) corresponding to the dust properties in the solar neighborhood. Classical big dust grains control the dust mass, where as small grains when present in an annulus, control T_d . Thus for the purposes of deriving dust mass, it is necessary to use the values of T_d appropriate to big grains only in Eq. 2. Details of the procedure followed in estimating such a T_d are discussed in Sec. 3.3.

The routines under Image Reduction and Analysis Facility (IRAF) and Space Telescope Science Data Analysis System (STSDAS) are used in the reduction and the analyses of the data.

3. Distribution of warm dust temperature

3.1. Radial profiles

As described in the previous section, the warm dust temperature (T_d) profiles are obtained from 60 and $100\mu\text{m}$ profiles assuming a λ^{-1} emissivity law. Resultant radial profiles for all the 22 galaxies are given in Fig. 1. Radial distances are expressed in units of optical isophote radius (R_{25}). The same temperature range is used in all the plots to enable easy comparison of absolute values as well as gradients from galaxy to galaxy. The solid line passing through the circles denotes the azimuthally averaged profiles, sampled at $1'$ intervals. The horizontal dotted line denotes the mean dust temperature of the galaxies as derived from

the global data. The following general trends can be noticed from these profiles.

1. In the inner half of the galaxy, the warm dust temperature decreases as one goes radially outwards from the center in a majority of the galaxies. The decrease is less than 3 K in galaxies NGC 628, 2403, 2841 and 7331, and more than 10 K in galaxies NGC 2903, 3079, 3628, 4258, 4535, 4736, 5033 and 6946. In the remaining 10 galaxies, T_d decreases by around 5–10 K.
2. Beyond half the disk radius, T_d shows a tendency to increase in about 50% of the cases.
3. The warm dust temperatures derived from global data are nearly the same as those for the high intensity inner regions.

The slightly poorer resolution of the $100\text{-}\mu\text{m}$ images as compared to the $60\text{-}\mu\text{m}$ images, may result in over-estimation of the central T_d . However the result (3) above, stating that the central T_d is not very much higher than the global T_d , indicates that the T_d is not severely affected by the difference in resolution of the two images. This indicates that the bulk of the FIR emission originates in regions which are much smaller than the beams in both the bands. This is consistent with the picture that the nuclear star forming regions and/or the bulge stars power the FIR emission.

3.2. Discussion on the heating sources

There has been a lot of discussion regarding the nature of heating sources of dust traceable by IRAS observations (see e.g. Devereux et al. 1994). The debate is on the fraction of heating provided by the non-ionizing photons from low to intermediate mass stars, which populate the disk of galaxies as against the heating by the Lyman continuum photons from the massive stars. Recent studies of M 31, M 101 and M 81 have revealed good positional coincidences between the $\text{H}\alpha$ and FIR emitting sources (Devereux et al. 1994; Devereux & Scowen 1994; Devereux et al. 1995), indicating that the massive stars when present

act as efficient heating sources. The $1'$ resolution in the present study corresponds to a linear size of 1–6 kpc in the program galaxies, which is larger than the extent of a typical star forming complex. Thus the observed T_d corresponds to a mixture of several populations. However the vastly differing heating efficiencies of ionizing and non-ionizing photons can be used to study the heating capabilities of old stars, which is the topic of discussion in the remaining part of this section.

We first compute the amount of heating by the interstellar radiation field (ISRF), which is mainly originating from long-lived low and intermediate mass stars. We use the calculations of Désert et al. (1990), who computed the expected flux densities within the IRAS bands for an assumed dust composition and spectrum of the heating radiation field. The dust composition chosen was such that it reproduces the galactic interstellar extinction curve (Savage & Mathis 1979), and contains Very Small Grains (VSGs), Polycyclic Aromatic Hydrocarbons (PAHs) in addition to the conventional Big Grains (BGs). They assumed the spectrum of the heating radiation field to be similar to that of the local interstellar radiation field (LISRF). The resulting flux densities in the IRAS bands (normalized to total hydrogen column densities) were tabulated as a function of the radiation field intensity in the V -band for each component of dust. They also computed the IRAS flux densities for ultraviolet enriched (with respect to LISRF) input radiation field by adding to the LISRF a component denoted as X_{uv} ($X_{uv} = 0$ and 3 correspond to LISRF and 3 times UV enriched LISRF respectively).

The models of Désert et al. can be used to compute the expected T_d gradients in galaxies, if V -band surface brightness profiles are known. For 13 of the program galaxies such data are available in a recently compiled data base (Frei et al. 1996), based on the observations at the Palomar Observatory. We assumed their CCD g -band ($\lambda 5000/700$) images to represent

the V -band surface brightness, and obtained V -band surface brightness profiles using methods identical to that followed in extracting 60 and $100\mu\text{m}$ profiles (Sec. 2). The ISRF as seen by the dust particles differs from the observed V -band surface brightness, due to the extinction by dust within the parent galaxy. The amount of visual extinction can be estimated using the observed gas density (N_H) along with the galactic value for A_v/N_H ($A_v/N_H = 5.3 \times 10^{-22} \text{ cm}^2$; Bohlin et al. 1978). Using A_v to estimate the ISRF from the observed optical surface brightness may be an upper limit as some of the scattered photons recombine to the observed surface brightness. Also only those dust particles in the foreground of stars will contribute to extinction and hence effectively only half the amount of particles might be contributing to extinction. Accordingly, we correct the V -band surface brightness profiles by A_v as estimated from $N_H/2$. N_H includes both the atomic and molecular contributions and were taken from the sources listed in Table 1.

The modeled T_d profiles for the 13 galaxies with optical CCD data are plotted in 13 panels of Fig. 2, along with the azimuthally averaged observed profiles. Open circles represent the observed T_d profile. Four models are shown by different line types which are identified in the last panel. Three of these correspond to the same dust mixture (VSG+PAH+BG), but for three different heating spectra, while the fourth one (dashed line) corresponds to the case where the ISM contains only the classical big grains. The solid and dash-dotted lines use the LISRF spectrum with ($X_{uv} = 3$) and without ($X_{uv} = 0$) UV enrichment respectively. For these two models the observed V -band profiles are corrected for the extinction as described above. For the third model (dotted line) $X_{uv} = 3$, but the observed V -band surface brightness profile is used ($A_v = 0$). The heating spectrum for the fourth model is identical with the third model and hence the contribution of the VSGs+PAHs (which increases with radius) can be inferred by comparing the dotted and

dashed lines. On the other hand, the difference between the solid and dotted lines illustrate the effect of the extinction, which is found to be significant in the central regions of galaxies. The difference between the solid line and the dash-dotted line (which is around 3–4 K) shows the effect of enhancement in the UV part of the heating spectrum.

With the chosen range of parameters related to the dust composition, heating radiation field and extinction, models encompass the observed range of T_d in a majority of the galaxies. We now select the models which best match the observed T_d profile in individual galaxies. The most obvious trend in the observed T_d profiles is the initial fall and the outward increase, which is fairly well reproduced by the models having a dust mixture containing PAHs and VSGs in addition to BGs. With only BGs, T_d is expected to monotonically decrease with distance from the center in all the galaxies. VSGs control the T_d in the outer disk, where the radiation intensity is low, whereas BGs do the same in the inner disk. However the amount of heating provided by the old stars with a spectrum similar to that of the LISRF ($X_{uv} = 0$) is found to be adequate to heat the dust to the observed T_d only in NGC 4501 and 5055. In the remaining galaxies, better results are obtained by using a spectrum with an enhanced UV continuum, which mimics the addition of young massive stars. It is expected that the UV contribution is not the same at all radial distances. However, we use a single X_{uv} value for all radii in order to show the role of this parameter in heating the dust. UV enhancement of a factor of three is found to be sufficient at most radial positions in seven of the remaining eleven galaxies (NGC 2903, 4254, 4258, 4303, 4321, 4535, 5033) studied here. In NGC 2403 & 3198, the observed T_d is around 5 K hotter than the ISRF heating models with $X_{uv} = 3$ in most parts of the disks. The observed T_d value in the central region of NGC 4535 is around 8 K hotter than the $X_{uv} = 3$ model, implying the necessity of an additional heating

source. The observed T_d is high in the outer regions of NGC 4569. The errors on T_d are also expected to be higher in this galaxy due to the combined effects of lower flux and poorer resolution compared to other galaxies in the sample. Thus the higher T_d in NGC 4569 may not be physically significant.

$X_{uv} = 3$ corresponds to a value less than 0.5% of stellar mass in the young stars as compared to the old stars per surface area, for a galaxy like the Milky Way as modeled by Bruzual & Charlot (1993). For a typical disk surface density of $10^7 M_\odot \text{ kpc}^{-2}$, this corresponds to $5 \times 10^4 M_\odot \text{ kpc}^{-2}$ in young stars. Giant HII regions in galaxies have typically a mass of $10^5 M_\odot$ in less than 1 kpc^2 area (Mayya & Prabhu 1996). Thus $X_{uv} = 3$ can be easily satisfied locally where giant HII regions are present. However, the observed number of giant HII regions in galaxies is insufficient to maintain a global $X_{uv} = 3$. The heating provided by the ionizing photons and Lyman alpha photons, which are not accounted by the X_{uv} parameter in Désert et al., are essential to explain the global heating.

Models with the extinction corrected ISRF predict a steep increase of T_d towards the center, which matches well the observed T_d gradients in NGC 2903 and 4192. In most of the remaining galaxies, the estimated extinction over-corrects the ISRF, thus resulting in higher model values of T_d in the central regions. While models without the UV contributing massive stars in the central regions can explain the central T_d gradients in some cases, the possible range of uncertainties in the estimation of A_v can as well reproduce the observed flatter gradients. We here point out that the extinction estimation in the central regions based on the observed gas density, which is dominated by H_2 , is likely to be uncertain due to our poor understanding of the dependence of gas-to-dust ratio, and the CO intensity to molecular hydrogen mass conversion factor, with metallicity. Fortunately, the two dependences are in the opposite directions and hence only the difference in their degree of dependences af-

fects the extinction estimation. These issues are re-addressed later in Sec. 4.2.

It is interesting to note that the dust heating models with a spectrum similar to that of LISRF correctly reproduce the observed shape of the T_d gradient, though it is cooler by around 5 K in majority of the galaxies. We found that, with the dust mixture assumed by Désert et al., the required additional heating can be provided by the UV photons from young stars in giant HII regions. However there are a few cases, like the outer region in NGC 2903, and over most of the radial extent in NGC 2403 and 3198, where the assumed range of parameters do not produce the observed T_d gradients. Increasing X_{uv} beyond 3 may result in a better match, but it is not consistent with the lack of massive stars in the outer region of NGC 2903. On the other hand it is likely that the VSG content in the dust mixture varies from region to region in galaxies and also from galaxy to galaxy. For e.g. Xu & Helou (1994) have found deficiency of VSGs in the ISM of M31, compared to that used by Désert et al. The observed higher T_d in the outer regions of the above galaxies may be due to a higher VSG content. Accordingly, we doubled the flux contributed by the VSGs at 60 & 100 μm , and recomputed the resulting T_d for the new dust mixture in galaxies NGC 2403, 2903 and 3198. The results of this study are plotted in Fig. 3. The open circles and the solid line have the same meaning as in Fig. 2. The dotted line has the same parameters as for the solid line, but for the enhanced VSG content. The plots illustrate that the high observed values of T_d can be explained in terms of enhanced VSG content in the dust mixture. Thus we conclude that the enhancement of the VSG content over that used by Désert et al. is required at least in some galaxies in the sample. More elaborate models, incorporating the heating provided by the ionizing photons as estimated from the observed $H\alpha$, in addition to the heating by the ISRF are required to reproduce the

observed T_d distribution for individual galaxies at all radii. Such studies will be instructive on the possible variations in the relative amounts of the three components of dust in the ISM. However, we continue to use the dust composition used by Désert et al. in the remaining part of this study.

3.3. Contribution from big grains alone to the computed quantities

For some applications (such as the optical depth, to be discussed in the next section) it is important to get an estimate of the contributions from big grains alone in the IRAS bands. Our analysis of the previous sub-section, based on the Désert et al. (1990) models, allows us to compute this contribution. We obtain the radial gradients of the 60 and 100 μm emission expected from the big grains alone in five of the largest (in angular size) galaxies in our sample. The results are plotted in the top two panels of Fig. 4, as fractions of the total (BG+VSG+PAH) emission in the respective bands. In obtaining these fractions, we have assumed the $X_{uv} = 3$ models after correcting for extinction based on estimated A_v (solid line in Fig. 2). It is interesting to note that the radial dependence is similar in the five galaxies studied, and hence the results from these plots may be extended to other galaxies too. The big grain contribution to the 60 μm emission falls below 50% beyond half the disk radius, reaching values as low as 20% at $0.8R_{25}$. In comparison the 100 μm emission is less affected by emission from VSGs+PAHs, contributing in the range of 15–25% beyond half the disk radius. As we saw in the previous sub-section, this differential contribution to the 60 and 100 μm bands affects the derived dust temperature the most. In the third panel of Fig. 4, we plot the T_d expected from the big grains alone as a fraction of the observed T_d for the same five galaxies as in the earlier panels. Again each of the five galaxies show very similar behavior. In the last panel a similar plot is given for $\tau_{60}(\text{BG})/\tau_{60}(\text{Obs})$, where the numerator is computed using $T_d(\text{BG})$ and $S_{60}(\text{BG})$

in Eq. 2. In the outer regions, the observationally derived τ_{60} is an order of magnitude lower compared to that expected from the big grains alone. This is due to the VSGs+PAHs affecting the τ_{60} indirectly through the steep T_d dependence (see Eq. 2). $\tau_{60}(\text{BG})$ can be obtained from the observationally derived τ_{60} by applying mean correction factors of $-0.05, 0.08, 0.37, 0.80, 1.25$ dex at radii 0.10, 0.25, 0.50, 0.75 and 1.00 R_{25} respectively. These values will be used to estimate Σ_d without the contaminating effects of VSGs and PAHs.

4. Distribution of τ_{60} and implications

At the FIR wavelengths the dust is optically thin to its own radiation and hence the amount of dust along the line of sight can be estimated from the observed FIR flux densities. Eqs. 2 and 3 in Sec. 2 define the $60\mu\text{m}$ optical depth, τ_{60} , and the dust surface mass density, Σ_d . The radial distribution of dust mass and the gas-to-dust ratio in galaxies are the subject of discussion in this section.

4.1. Radial gradients

τ_{60} profiles for all the galaxies are computed following Eq. 2, making use of the azimuthally averaged $60\mu\text{m}$ intensity profiles and T_d profiles discussed in the previous section. The resultant profiles (in log units) are plotted in Fig. 5 as a function of the radial distance from the center in units of optical disk radius. The open circles denote the observed τ_{60} profile, whereas the filled circles (in 13 galaxies where we have modeled the T_d gradient) represent the expected τ_{60} from big grains alone, following the discussions in Sec. 3.3. It should be noted that VSG and PAH contribute very little to the derived dust mass density; it is mostly $\tau_{60}(\text{BG})$ that is a measure of the dust mass density, and thus we refer $\tau_{60}(\text{BG})$ as the corrected τ_{60} henceforth. The various curves plotted in Fig. 5 correspond to the values estimated from the observed gas density profile, which are discussed in detail be-

low.

The observed τ_{60} in general increases as radius decreases; in the central region it shows a tendency to flatten off or dip downwards. Such trends were also noticed earlier by Ghosh et al. (1993) in a study based on maximum entropy deconvolution of IRAS images. The observed τ_{60} profiles become flatter after correcting them using Désert et al. model. There are two galaxies — NGC 4192 and 4501 in which the corrected τ_{60} increases with radius. Subtraction of the VSG and PAH contribution based on the model of Désert et al. (1990) are over-corrections for these galaxies as can be inferred from the T_d plots (Fig. 2). The actual values may be intermediate to the two sets. It may, however, be noted that the observed τ_{60} profile increases with radius in NGC 3628 and is almost flat in NGC 3079. These are the only two sample galaxies which are within 15° of being edge-on, and may need a separate treatment.

In order to understand the general behavior of τ_{60} decreasing radially outwards, we look into the various factors controlling the optical depth at FIR wavelengths. For a given value of the gas-to-dust ratio, τ_{60} mainly depends on the scattering properties of the dust mixture and total column density of the gas (N_H). It is likely that the gas-to-dust ratio itself depends on the metallicity (Z) in the galaxy. Thus the optical depth at a FIR wavelength λ can be written as,

$$\tau_\lambda = 0.921 \left(\frac{A_V}{N_H} \right) \left(\frac{Z}{Z_\odot} \right)^b N_H \left(\frac{A_\lambda}{A_V} \right), \quad (4)$$

where b is the power law index to take into account of a possible dependence of the gas-to-dust ratio with metallicity. Substituting the galactic value of A_V/N_H , and expressing N_H in terms of the mass surface density Σ_H , we get,

$$\tau_{60} = 3.66 \times 10^{-2} \left(\frac{\Sigma_H}{M_\odot \text{pc}^{-2}} \right) \cdot \left(\frac{Z}{Z_\odot} \right)^b \left(\frac{\tau_{60}}{\tau_V} \right), \quad (5)$$

where $\frac{\tau_{60}}{\tau_V}$ is the relative optical depth, which can vary over a large range depending on the shape of the

extinction curve. Casey (1991) has determined the τ_V/τ_{60} values to be in the range 800–4000 for clouds in the vicinity of hot stars and 150–700 towards cooler molecular clouds. The effective τ_V/τ_{60} is determined by the size distribution of the dust particles and the effective wavelength of the radiation field.

The computation of τ_{60} requires a knowledge of the gradients in the gas surface density, metallicity and τ_V/τ_{60} as well. The gas surface densities are dominated by the molecular hydrogen, as traced by the CO line in the central regions and the neutral hydrogen in the outer regions. Observational data both in atomic and molecular phases are available for the program galaxies in the literature. The last two columns in Table 1 list the sources of these data. The CO line intensity to H₂ mass conversion factor is expected to be a function of Z; at present we follow the conventional method, but consider the Z-dependence later in Sec. 4.2. Metallicity decreases radially outwards in galaxies. In a recent study, Zaritsky et al. (1994) find that the absolute value of metallicity as well as the gradient vary over a wide range between different galaxies, which are found to correlate with the Hubble type, luminosity and the presence or the absence of a bar. Abundance gradients in 13 galaxies of our sample are available in Zaritsky et al. (1994), which are listed in Table 1. For the rest of the galaxies we assume a gradient of 0.05 dex/kpc normalized to the solar metallicity at a radial distance of 10 kpc from the center. These assumed values closely match the observed values for NGC 628, 2903, 5055 and 6946. Dust heating models by Casey (1991) reveal that τ_V/τ_{60} increases with increasing effective temperature of the heating stars and decreasing effective grain size. Effective temperatures of stars of a given mass are expected to be higher at the low metallicity found in the outer galaxies (Cerviño & Mas-Hesse 1994). The low radiation field intensity at the outer radii favors the survival of VSGs, thus resulting in the effective decrease of grain size with radius; the observed T_d gra-

dients also support the presence of significant amount of VSGs at the outer radius. Thus we expect an increase in τ_V/τ_{60} with radius. However because of the uncertainties involved in expressing this gradient, we prefer to fix it at a given value for each galaxy and comment on its effect on the observed τ_{60} gradient.

The τ_{60} profiles are obtained for all the galaxies, based on the observed gas density profiles and Eq. 5, and are plotted in Fig. 5. The solid and dotted lines correspond to the computed τ_{60} for $\Sigma_H = \Sigma_{HI} + \Sigma_{H_2}$ and $\Sigma_H = \Sigma_{HI}$ respectively, with $b = 1$. The effect of neglecting the dependence of gas-to-dust ratio on Z, i.e. $b = 0$ in Eq. 5, is shown by the dashed line. There is one panel for each galaxy, with an additional panel at the end explaining the different line types used. The values of τ_V/τ_{60} are chosen such that the computed τ_{60} profile matches the observed profile shape, over the maximum radial extent. The resulting values are indicated on the plots. It should be noted that the absolute values of τ_V/τ_{60} are based on the assumption of a constant gas-to-dust ratio from one galaxy to another. The observed data can be equally well matched by fixing τ_V/τ_{60} at the galactic value and allowing the gas-to-dust ratio to vary from galaxy to galaxy. From an inspection of Fig. 5, we can make the following general comments. In most galaxies, the τ_{60} profile computed from H₂ or total gas rises as one goes to the center, whereas the profile computed from HI alone even with Z dependence is much flatter. The observed profile rises towards the center in only 8 galaxies. The observed profiles more often match the computed profile for either HI with Z dependence or the total gas with no Z dependence which is flatter. If we consider only the sample of 13 galaxies for which VSG corrections are available (filled circles in Fig. 5), none shows a match with total gas with Z dependence $b = 1$; four each match with only HI with Z dependence and total gas with no Z dependence. In 3 galaxies no gas profile can give a reasonable fit.

4.2. Spatial variation of gas-to-dust mass ratio

In the previous subsection we investigated the various factors responsible for the variation of the $60\mu\text{m}$ optical depth in individual galaxies. For a constant gas-to-dust ratio in galaxies, the observed range of τ_{60} implies τ_V/τ_{60} variations over a factor of ten in different galaxies. This factor can be marginally reduced by invoking the gas-to-dust ratio to vary inversely with metallicity. However it is conventional to derive dust masses in galaxies by fixing the values of τ_V/τ_{60} corresponding to the dust properties in the solar neighborhood. For a gas-to-dust mass ratio of 160, Eq. 2 and 3 imply a value of $\tau_V/\tau_{60} = 600$.

We derive the profiles of the gas-to-dust ratio in galaxies by dividing the observed profiles of gas surface density by the dust surface density. The resulting variation of the gas-to-dust ratio with radial distance from the center, expressed in units of optical radius, is shown in Fig. 6. Distributions of $\Sigma_{\text{HI}}/\Sigma_{\text{d}}$, $\Sigma_{\text{H}_2}/\Sigma_{\text{d}}$ and $(\Sigma_{\text{HI}}+\Sigma_{\text{H}_2})/\Sigma_{\text{d}}$ are shown separately. At each radius there is one open circle for each galaxy. The sampled radii correspond to 10, 25, 50, 75 and 100% of the disk radius. The median values are shown joined by a solid line. The dotted line is the median line after applying the estimated correction factors listed in Sec. 3.3 for the subtraction of contributions from VSGs and PAHs. With the adopted corrections, the dust mass increases by factors of 1.2, 2.3, 6.3 and 17.8 at 25, 50, 75 and 100% of the disk radius respectively. In the inner regions the total gas mass is predominantly molecular and in the outer regions, it is mostly HI. The corrected radial profile of the gas-to-dust ratio is almost flat for the HI alone, and decreases with radius for the H_2 and total gas. For the total gas profile, the gas-to-dust ratio at $R=R_{25}$ is about 215, very close to the local Milky Way value, but increases by a factor of 8 at the center. This smooth gradient is unlikely to represent the real gas-to-dust mass variations and hence we investigate possible sources for

this large scale gradient.

We first consider the effects of metallicity. It is conventional to derive the column density of molecular hydrogen from the CO line intensity using a factor, $X = 2.8 \times 10^{20} \text{ cm}^{-2}/(\text{K km s}^{-1})$, independent of metallicity of the region (Young et al. 1989). Attempts to estimate X in external galaxies have revealed X to be dependent on metallicity. For example the best estimated values of X in the low metallicity systems the Large and Small Magellanic Clouds are respectively 6 and 20 times larger than the usually assumed value (Cohen et al. 1988; Rubin et al. 1991). Nakai & Kuno (1995) also find higher values of X in the lower metallicity outer region of M 51. Arimoto et al. (1996) have compiled the estimates of the conversion factor at different metallicities using data from several galaxies and find that the conversion factor X is inversely proportional to Z . Following this most recent study, we take

$$N_{\text{H}_2}(\text{true}) = N_{\text{H}_2}(\text{CO})z^{-a}, \quad (6)$$

where $z = Z/Z_{\odot}$. The dependence of the gas-to-dust ratio with metallicity can also be taken as a power law, z^b . Taking $a = 1$ (Arimoto et al. 1996), we then consider two extreme cases $b = 1$ and $b = 0$. We then expect for $b = 1$,

$$\frac{z\Sigma_{\text{HI}} + \Sigma_{\text{H}_2}(\text{CO})}{\Sigma_{\text{d}}} = \text{constant}, \quad (7)$$

and for $b = 0$,

$$\frac{\Sigma_{\text{HI}} + \Sigma_{\text{H}_2}(\text{CO})/z}{\Sigma_{\text{d}}} = \text{constant}. \quad (8)$$

In Fig. 7, we plot the gas-to-dust ratio for the individual gas components as well as the total, for both cases, $b = 1$ (panels to the left), and $b = 0$. The points and the solid lines show the values in individual galaxies and their median at the 5 selected radii for the 13 galaxies with metallicity data from Zaritsky et al. (1994). Dotted lines represent the median values after correction for the contamination from VSG+PAH. It

can be seen that the corrected gas-to-dust ratio remains much flatter all along the disk if the conversion factor X varies inversely with z (i.e. $a = 1$; Arimoto et al. 1996), and the dust fraction does not depend on metallicity ($b = 0$). For this curve, the corrected gas-to-dust ratio beyond half the disk radius is around 300, increasing to only about 650 at the center.

The derived absolute value of the gas-to-dust ratio depends on many uncertainties like the absolute value of X , its dependence with z , the FIR dust emissivity and the contribution of VSG and PAH to the FIR emission and the resultant correction to τ_{60} etc. In the present study we have shown that the gradient in the gas-to-dust ratio is very sensitive to the corrections to all the above effects. With our most realistic corrections, the gas-to-dust ratio in the outer galaxies turns out to be not very much different from the local Galactic value of 160. However, the central value is still higher by factor of 3–4. This can arise from the fact that while in the outer regions, the gas is predominantly diffuse HI and is less dense, in the inner region, it is molecular, which is denser and more clumpy. Not all the dust associated with the molecular gas would then be heated to the warm temperature detectable by IRAS. Recent studies of normal “in-active” galaxies using mm continua indicate temperatures ranging from 10–20 K for the cold dust (Chini et al. 1995), consistent with our results. Sub-mm observations with the Infrared Space Observatory (ISO), with its capability for high angular resolution, will have a major role to play in elucidating the role of cool dust and its location in galaxies.

4.3. Global gas-to-dust ratio

Young et al. (1989) investigated correlations between the global dust mass and neutral and molecular hydrogen, and came to the conclusion that the IRAS-detected dust is closely associated with the molecular gas. The radial profiles of the optical depth of our sample galaxies are systematically flatter than that of

H₂, implying that the dust is not preferentially associated with the molecular gas locally within galaxies. We carry out the following analysis to sort out this apparent discrepancy. Cumulative dust and gas masses in our program galaxies are computed by summing over the radial profiles of dust and gas distribution. The resultant gas-to-dust mass ratios are plotted in Fig. 8 as a function of the fractional disk radius (3 panels on the left). The open circles and the solid lines have the same meaning as in Fig. 6. The dotted lines represent cumulative values after using the corrected dust and recomputed molecular ($a = 1$) masses. We use $b = 0$ following the results from Fig. 7. Only 13 galaxies with the metallicity data are used in these plots. From this figure it is noted that the dispersion close to the center is larger for both HI and H₂ than in the outer (global) regions. For the global value ($R/R_{25} = 1$), the dispersion is again similar for HI and H₂. Thus we find that the dust mass is equally well correlated with both the HI and H₂ gas for this small sample. The presence of a non-negligible HI mass outside the optical radius may be the reason for the relatively poor correlation between global dust and HI masses as seen by Young et al. (1989).

The global value of 300 for the gas-to-dust ratio is, within a factor of two, the same as the canonical value. Note that the global value is representative of the outer disk rather than the higher intensity inner disk value of 600, contrary to the general belief. Why it is so can be understood from the three panels on the right in Fig. 8. Cumulative masses of the total gas, molecular hydrogen and dust are plotted separately normalized by the respective global masses (at $R=R_{25}$). As in the previous plots open circles and solid lines show the observed masses, while the dotted lines show the corrected masses. The panel for the dust mass also includes the cumulative FIR luminosity (defined by the numerator of Eq. 1), again normalized by the total FIR luminosity. These plots reveal that the gas and dust lying outside half the disk

radius contribute as much as 60% to the total gaseous mass and dust mass. Thus outer regions control the global gas-to-dust ratio in galaxies.

The availability of radial profiles of dust and gas mass distributions gives us an opportunity to comment on the wide range of global gas-to-dust mass ratios reported in the literature. The most important results from this study on the gas and dust mass distributions are summarized in Table 2, to ease comparisons with other data sets. The corrected dust mass that we compute, based on the Désert et al. (1990) model, takes into account all the mass in dust particles hotter than 20 K. The dust masses derived from the global IRAS data are weighted by the FIR intensity, 90% of which comes from within half the disk radius, and hence pertain only to the central value. If we follow the usual practice of neglecting the Z -dependence of the CO intensity to H_2 mass conversion factor, we derive a value between 700–1350 (Col. 9), for the global gas-to-dust mass ratio. This explains the results from Devereux & Young (1990), who obtained a value of around 1000 using global IRAS data. Correcting the molecular masses for the effects of Z decreases the total gas mass by only around 20% (Col. 5), but drastically flattens the radial distribution of the gas-to-dust ratio (Cols. 7 and 8). Thus without these corrections, observed gas-to-dust ratios are expected to be highly aperture dependent even if the dust masses are determined using mm and sub-mm aperture observations, as illustrated in Col. 10. Andreani et al. (1995), using mm dust continuum observations and a X value reduced by 1.6 times, derive a global gas-to-dust ratio of 230, in good agreement with our corrected global value (Col. 11).

5. Conclusions

Gradients in the warm dust temperature within spiral galaxies are studied for a sample of 22 galaxies with low levels of present star formation. The observed T_d is found to decrease away from the center,

followed by a slow increase in the outer parts of galaxies. We invoked the Désert et al. (1990) models to estimate the heating of dust by non-ionizing photons from the bulge and disk stars in 13 of these galaxies. The model reproduces the observed T_d gradients qualitatively well, with very small grains playing a major role in maintaining high T_d values at regions of low flux levels such as in the outer regions of galaxies. However, additional heating sources from recent star forming events are required for a detailed matching of the T_d profiles. Correction for the contribution from very small grains is essential to derive the optical depth due to the big grains alone, which dominate the dust mass. Surface density profiles of dust are flatter than that of molecular hydrogen in nearly 50% of the galaxies, implying that only a part of the dust mass associated with the molecular hydrogen contributes to the FIR emission. We further showed that the often reported high values (~ 1000) for the gas-to-dust ratios in galaxies from global IRAS data, are due to a combination of over-estimation of molecular masses (as a result of using a metallicity-independent conversion factor from CO intensity to H_2 column density), and due to the presence of significant amounts of cool dust in the outer fainter parts of galaxies. When corrections are made for these effects, radial profiles of the gas-to-dust mass ratio flatten out, and the global value approaches, to within a factor of two, the local galactic value.

It is a pleasure to thank Dr. Walter Rice, the referee, for his comments and suggestions towards improvement of the manuscript. We wish to thank Dr. Z. Frei and collaborators for making their reduced CCD data of galaxies available for public use. This research has made use of the NASA/IPAC Extragalactic Database (NED) which is operated by the Jet Propulsion Laboratory, California Institute of Technology, under contract with the National Aeronautics and Space Administration.

REFERENCES

- Andreani, P., Casoli, F., & Gerin, M., 1995, *A&A* 300, 43
- Arimoto, N., Sofue, Y. & Tsujimoto, T., 1996, *PASJ* 48, 275
- Begeman, K., 1987, Ph.D. Thesis, University of Groningen, 106
- Bohlin, R.C., Savage, B.D., & Drake, J.F., 1978, *ApJ* 224, 225
- Bosma, A., 1978, Ph.D. thesis, University of Groningen, 30
- Bruzual, G.A., & Charlot, S., 1993, *ApJ* 405, 538
- Casey, S.C., 1991, *ApJ* 371, 183
- Cerviño, M., & Mas-Hesse, J.M., 1994, *A&A* 284, 749
- Chini, R., Krügel, E., 1993, *A&A* 279, 385
- Chini, R., Krügel, E., Lemke, R., & Ward-Thompson, D., 1995, *A&A* 295, 317
- Cohen, R. S., Dame, T. M., Garay, G., et al., 1988, *ApJ* 331, L95
- Désert, F.-X., Boulanger, F., & Puggè, J.L., 1990, *A&A* 237, 215
- de Vaucouleurs, G., de Vaucouleurs, A., Corwin, H.G., et al., 1991, *Third Reference Catalogue of Bright Galaxies*, (New York: Springer-Verlag)(RC3)
- Devereux, N.A., Scowen, P.A., 1994, *AJ* 108, 1244
- Devereux, N.A., Young, J.S., 1990, *ApJ* 359, 42
- Devereux, N.A., Jacoby, G., & Ciardullo, R., 1995, *AJ* 110, 1115
- Devereux, N.A., Price, R., Wells, L.A., & Duric, N., 1994, *AJ* 108, 1667
- Ghosh, S.K., Verma, R.P., Rengarajan, T.N., Das, B., & Saraiya, H.T., 1993, *ApJS* 86, 401
- Frei, Z., Guhathakurta, P., Gunn, J.E., & Tyson, J.A., 1996, *AJ* 111, 174
- Helou, G., Khan, I.R., Malak, L., & Boehmer, L., 1988, *ApJS* 68, 151
- Helou, G., Soifer, B.T., & Rowan-Robinson, M., 1985, *ApJ* 298, L7
- Hilderbrand, R.H., 1983, *QJRAS* 24, 267
- Irwin, J.A., Seaquist, E.R., 1991, *ApJ* 371, 111
- Kenney, J., & Young, J.S., 1988, *ApJS* 66, 261
- Mayya, Y.D., & Prabhu, T.P., 1996, *AJ* 111, 1252
- Mayya, Y.D., & Rengarajan, T.N., 1997 (Paper I)
- Nakai, N., & Kuno, N., 1995, *PASJ* 47, 761
- Rengarajan, T.N., & Verma, R.P., 1986, *A&A* 165, 300
- Rice, W., 1993, *AJ* 105, 67
- Rubio, M., Garay, G., Montani, J., & Thaddeus, P., 1991, *ApJ* 368, 173
- Savage, B.D. & Mathis, J.S., 1979, *ARA&A* 17, 73
- Sodroski, T. J., Bennett, C., Boggess, N., et al., 1994, *ApJ* 428, 638
- Tacconi, L., & Young, J.S., 1986, *ApJ* 308, 600
- Tully, B.R., 1988, *Nearby Galaxies Catalog*, Cambridge Univ. Press
- Walterbos, R.A.M., & Schwering, P.B.W., 1987, *ApJ* 287, L65
- Walterbos, R.A.M., & Greenawalt, B., 1996, *ApJ* 460, 696
- Warmels, R.H., 1988, *A&AS* 72, 427

- Wevers, B.M.H.R., van der Kruit, P.C., & Allen, R.J.,
1986, A&AS 66, 505
- Wilding, T., Alexander, P., & Green, D.A., 1993,
MNRAS 263, 1075
- Xu, C., & Helou, G., 1994, ApJ 426, 109
- Xu, C., & Helou, G., 1996, ApJ 456, 152
- Young, J.S., Xie, S., Kenney, J.D., & Rice, W.L.,
1989, ApJS 70, 699
- Young, J.S., Xie, S., Tacconi, L., et al. 1995, ApJS
98, 219
- Zaritsky, D., Kennicutt, R.C., & Huchra, J.P., 1994,
ApJ 420, 87
- Zhang, X., Wright, M., & Alexander, P., 1993, ApJ
418, 100

TABLE 1
BASIC DATA ON SAMPLE GALAXIES

NGC	Type	dist Mpc	S ₆₀ Jy	L _{fir} /L _B	60μm beam " x "	D' ₂₅	b/a	PA °	Z ¹	Z-grad dex/kpc	Ref	
											H I	H ₂
628	SA(s)c	9.7	25.5	3.41	77 x 42	10.47	0.91	25	9.13	-0.063	1	9
2403	SAB(s)d	4.2	62.6	2.04	60 x 42	21.88	0.56	127	8.80	-0.058	1	9
2841	SA(r)b	12.0	6.3	1.01	79 x 45	8.13	0.44	147	2	9
2903	SAB(rs)bc	6.3	67.6	3.70	68 x 45	12.59	0.48	17	9.22	-0.058	1	9
3079	SB(s)c	20.4	52.8	9.90	40 x 35	7.94	0.18	165	3	9
3198	SB(rs)c	10.8	6.9	1.43	67 x 32	8.51	0.39	35	8.94	-0.065	1	...
3627	SAB(s)b	6.6	66.5	4.22	72 x 42	9.12	0.46	173	4	9
3628	ScP	7.7	56.9	4.17	86 x 35	14.79	0.20	104	5	9
4192	SAB(s)ab	16.8	8.4	1.40	92 x 45	9.77	0.28	155	6	10
4254	SA(s)c	16.8	40.7	6.41	64 x 43	5.37	0.87	0	9.26	-0.035	6	10
4258	SAB(s)bc	6.8	27.4	1.16	63 x 43	18.62	0.87	150	9.07	-0.031	1	9
4303	SAB(rs)bc	15.2	40.2	6.01	83 x 45	6.46	0.89	0	9.20	-0.078	6	10
4321	SAB(s)bc	16.8	26.9	4.10	55 x 35	7.41	0.85	30	9.32	-0.012	6	10
4501	SA(rs)b	16.8	20.7	3.32	61 x 44	6.92	0.54	140	6	10
4535	SAB(s)c	16.8	12.6	2.52	62 x 44	7.08	0.71	0	6	10
4569	SAB(rs)ab	16.8	11.0	1.33	84 x 44	9.55	0.46	23	6	10
4736	RSA(r)ab	4.3	75.2	2.76	63 x 42	11.22	0.81	105	9.00	-0.025	7	9
5033	SA(s)c	18.7	21.6	3.99	65 x 43	10.72	0.47	170	9.09	-0.035	1	9
5055	SA(rs)bc	7.2	50.9	3.95	61 x 42	12.59	0.58	105	9.31	-0.058	1	9
6503	SA(s)cd	6.1	11.1	2.09	67 x 44	7.08	0.34	123	1	9
6946	SAB(rs)cd	5.5	165.2	2.87	39 x 35	11.48	0.85	32	9.13	-0.052	8	9
7331	SA(s)b	14.3	41.9	4.06	75 x 43	10.47	0.36	171	9.15	-0.024	2	9

¹12+log(O/H) at radius 3 kpc

REFERENCES.— (1) Wevers et al. 1986; (2) Begeman 1987; (3) Irwin & Seaquist 1991; (4) Zhang et al. 1993; (5) Wilding et al. 1993; (6) Warmels 1988; (7) Bosma 1978; (8) Tacconi & Young 1986; (9) Young et al. 1995; (10) Kenney & Young 1988

TABLE 2
MEAN PROPERTIES OF GAS AND DUST MASSES IN SAMPLE GALAXIES

R/R_{25}	f_{Σ_D}	f_{M_D}	$f_{M_{H_2}}$	f_{M_H}	Σ_H/Σ_D	Σ_H/Σ'_D	Σ'_H/Σ'_D	M_H/M_D	M_H/M'_D	M'_H/M'_D
1	2	3	4	5	6	7	8	9	10	11
0.1	0.90	1.00	0.30	0.35	1567	1761	655	1349	1318	575
0.5	2.34	1.55	0.54	0.76	955	408	274	692	501	316
1.0	17.78	2.75	0.54	0.79	3802	214	335	832	347	275

NOTE.— Col. 2: The adopted mean correction factor for dust mass at the three chosen radii, following the discussion in sec. 3.3.

Cols. 3–5: Ratios of the uncorrected to the corrected cumulative masses, for the dust, H_2 and the total gas respectively. Correction to H_2 mass involves the usage of metallicity dependent conversion factor between CO line intensity and H_2 mass.

Cols. 6–8: Gas-to-dust surface mass ratios at the three sampled radii, with primes denoting the quantities after corrections, following our prescriptions described above.

Cols. 9–11: Cumulative gas-to-dust mass ratios, with and without corrections. As in the earlier columns, primes indicate corrected quantities.

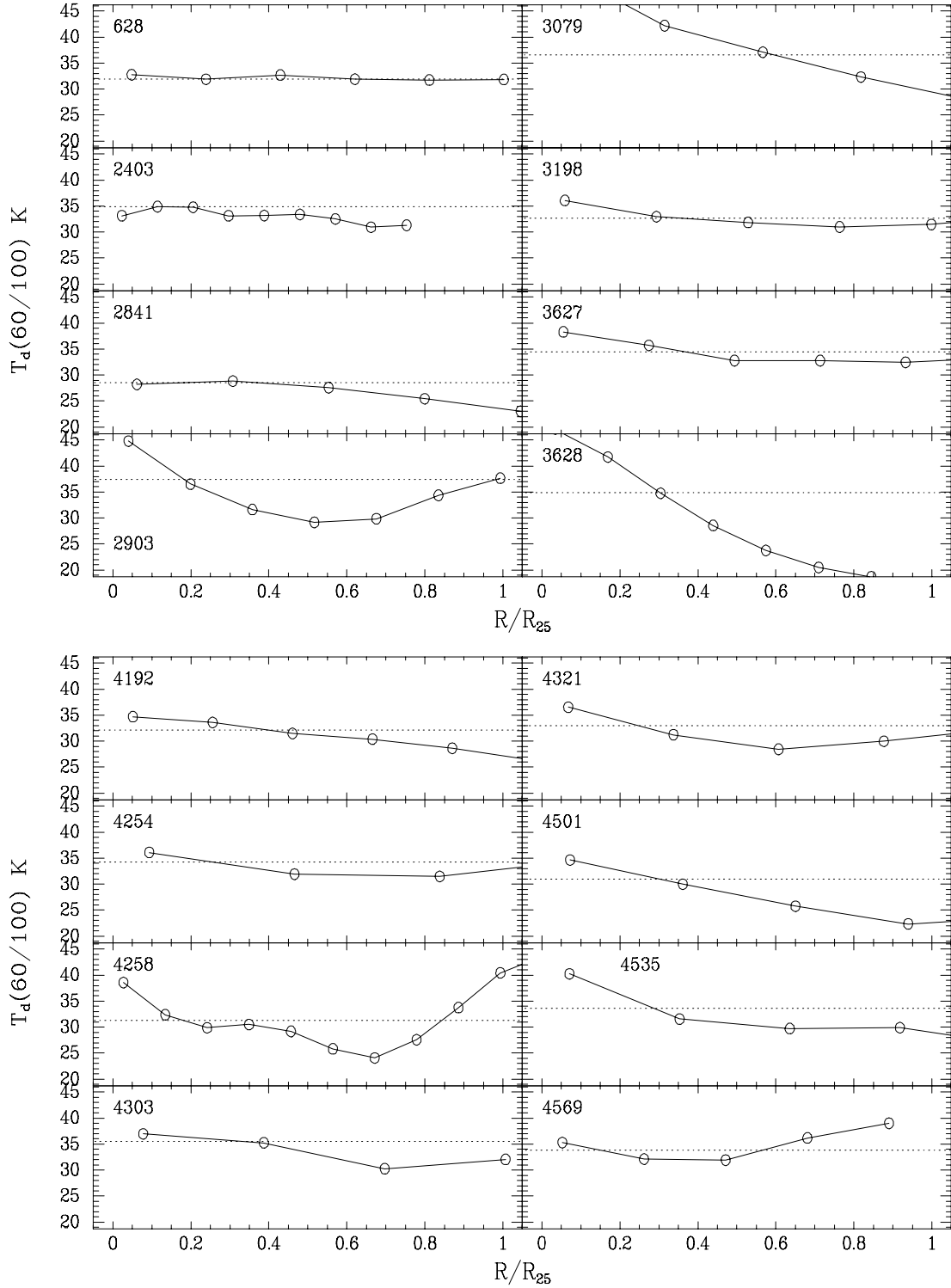


Fig. 1.— Observed warm dust temperature profiles (open circles at $1'$ intervals joined by the solid line) in 22 galaxies are plotted as a function of distance from the center, expressed in units of disk radius. NGC numbers of galaxies are given on the left side in each panel. The dotted lines correspond to the T_d values derived from the global data. The same range of T_d is plotted in all the galaxies to enable easy comparison of gradients and absolute values of different galaxies. T_d decreases away from the center increasing again by a few Kelvin at the outer radii in the majority of the galaxies.

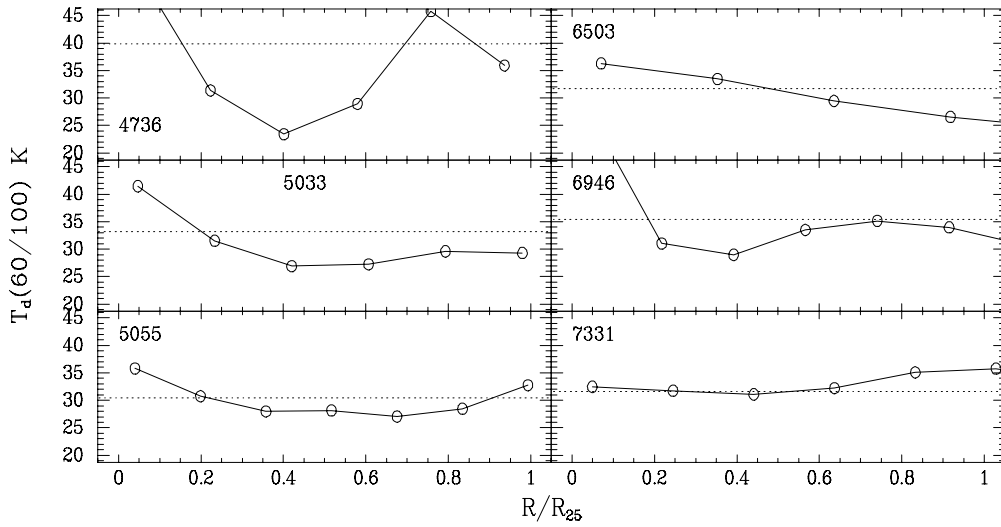


Fig. 1.— Continued.

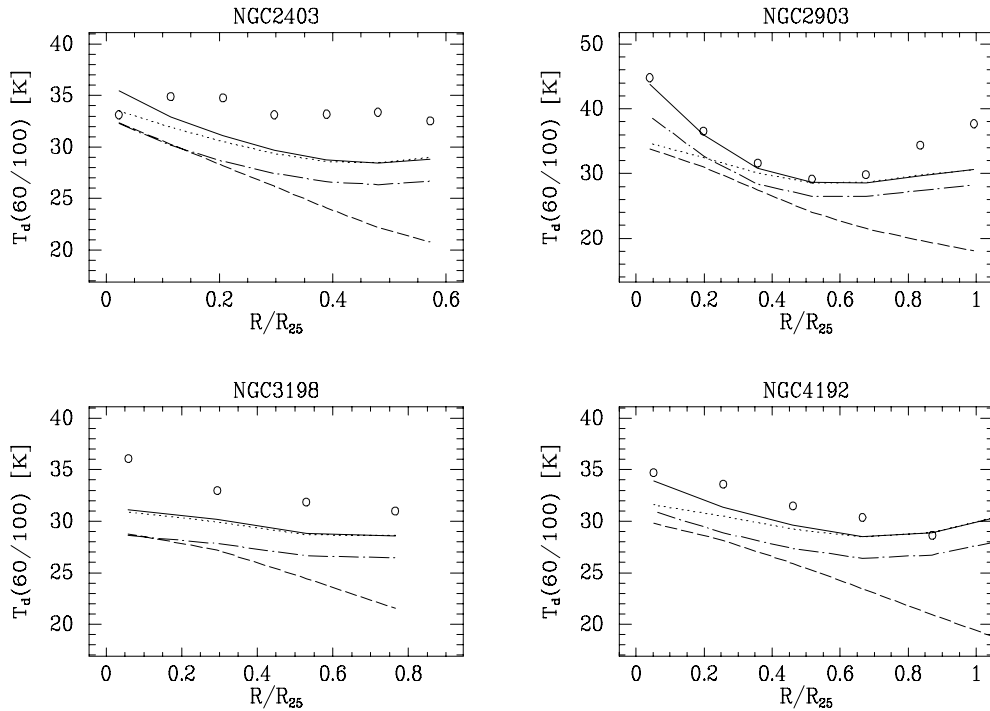


Fig. 2.— Observed T_d gradients in 13 galaxies are compared with the dust heating by the interstellar radiation field as modeled by Désert et al. (1990). The last panel explains the meaning of the different lines. The observed data points are denoted by the open circles. Note the importance of small grains (VSGs+PAHs) in reproducing the outward increase of T_d beyond half the disk radius in majority of the galaxies.

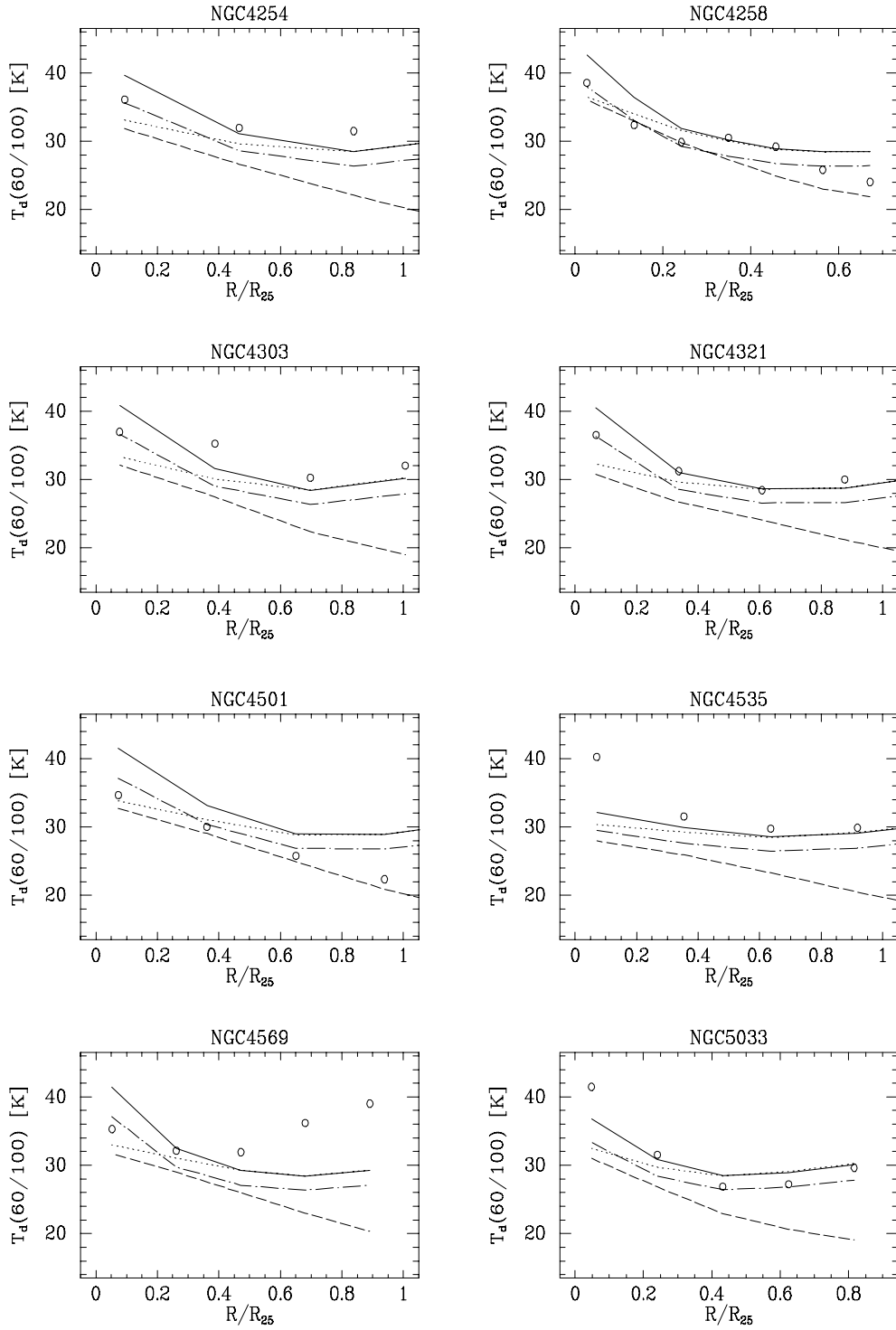


Fig. 2.— Continued.

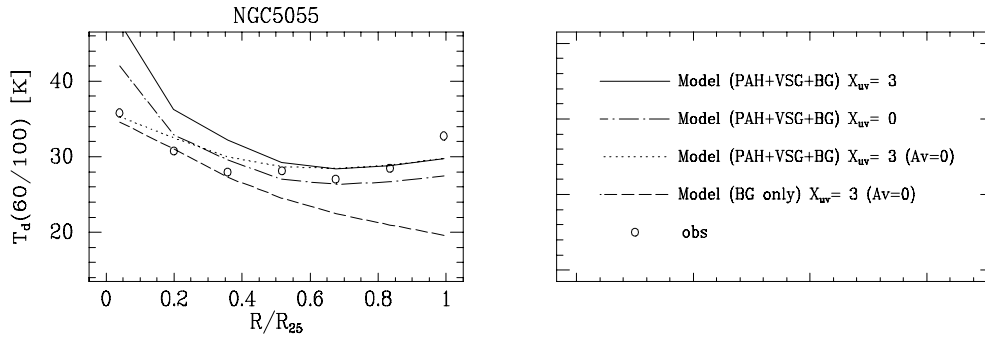


Fig. 2.— Continued.

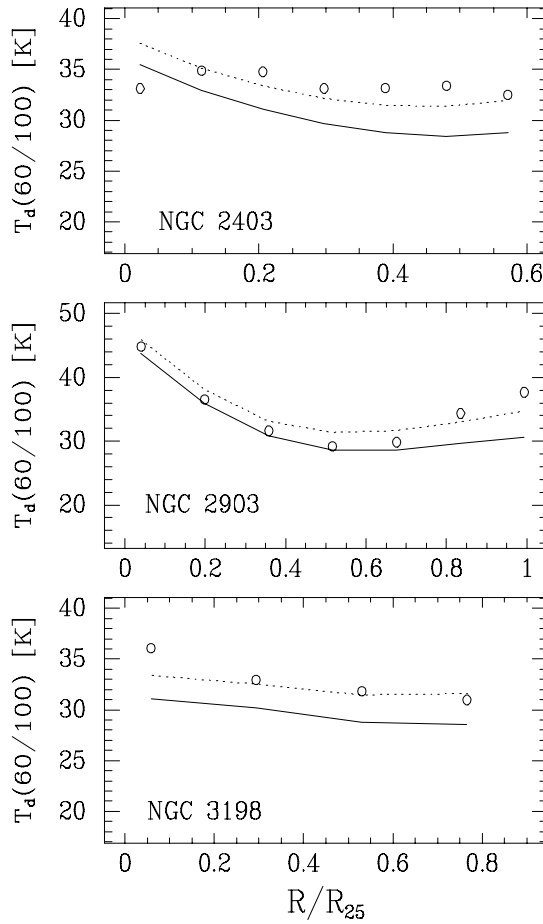


Fig. 3.— T_d radial gradients in three galaxies with the largest difference between the observed and modeled gradients are plotted. Open circles and the solid lines are the same as plotted in Fig. 2. The dotted line corresponds to a model, in which the flux contribution to the 60 and $100\mu\text{m}$ bands from VSGs are doubled with respect the values expected from the Désert et al. (1990) model.

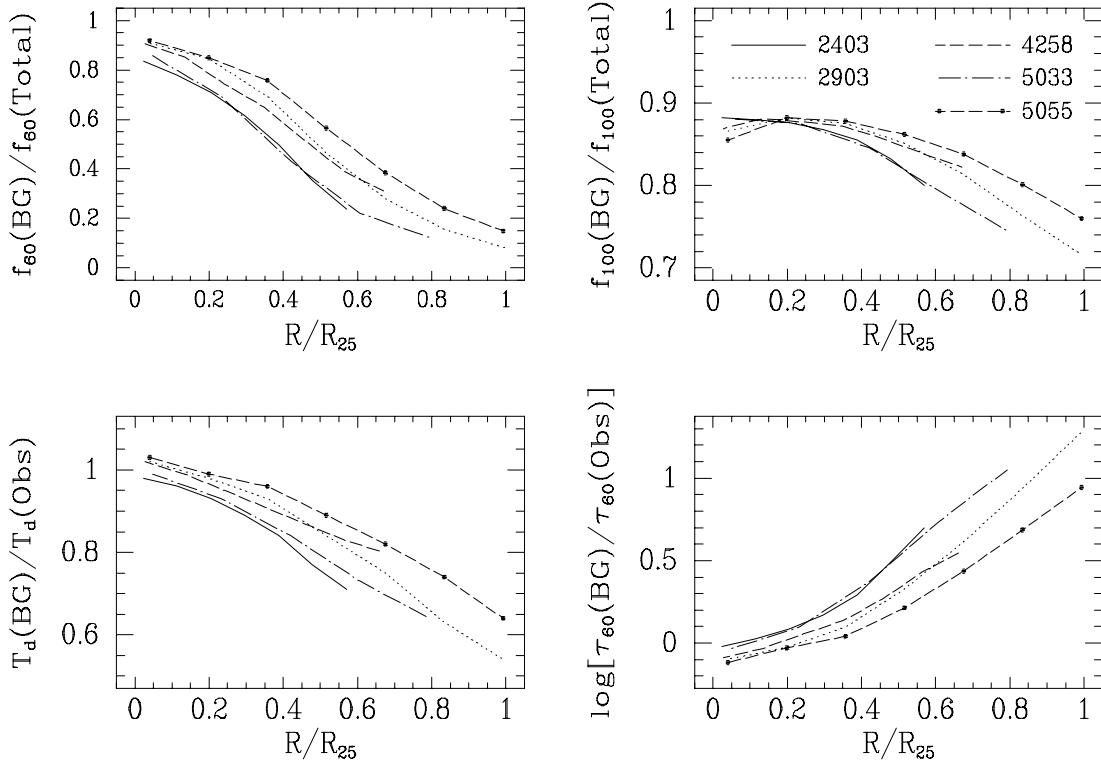


Fig. 4.— The contribution to the 60 and 100 μ m emission from the big grains alone, as fraction of the total emission, is plotted as a function of the radial distance for five representative galaxies in the sample in the top two panels. The dust temperature and optical depth are also computed taking into account the contribution from big grains alone and are plotted as fractions of the corresponding observed values, in the other two panels. The fact that all of the five galaxies show similar radial behavior, helps in estimating the contributions from the big grains alone in the rest of the galaxies.

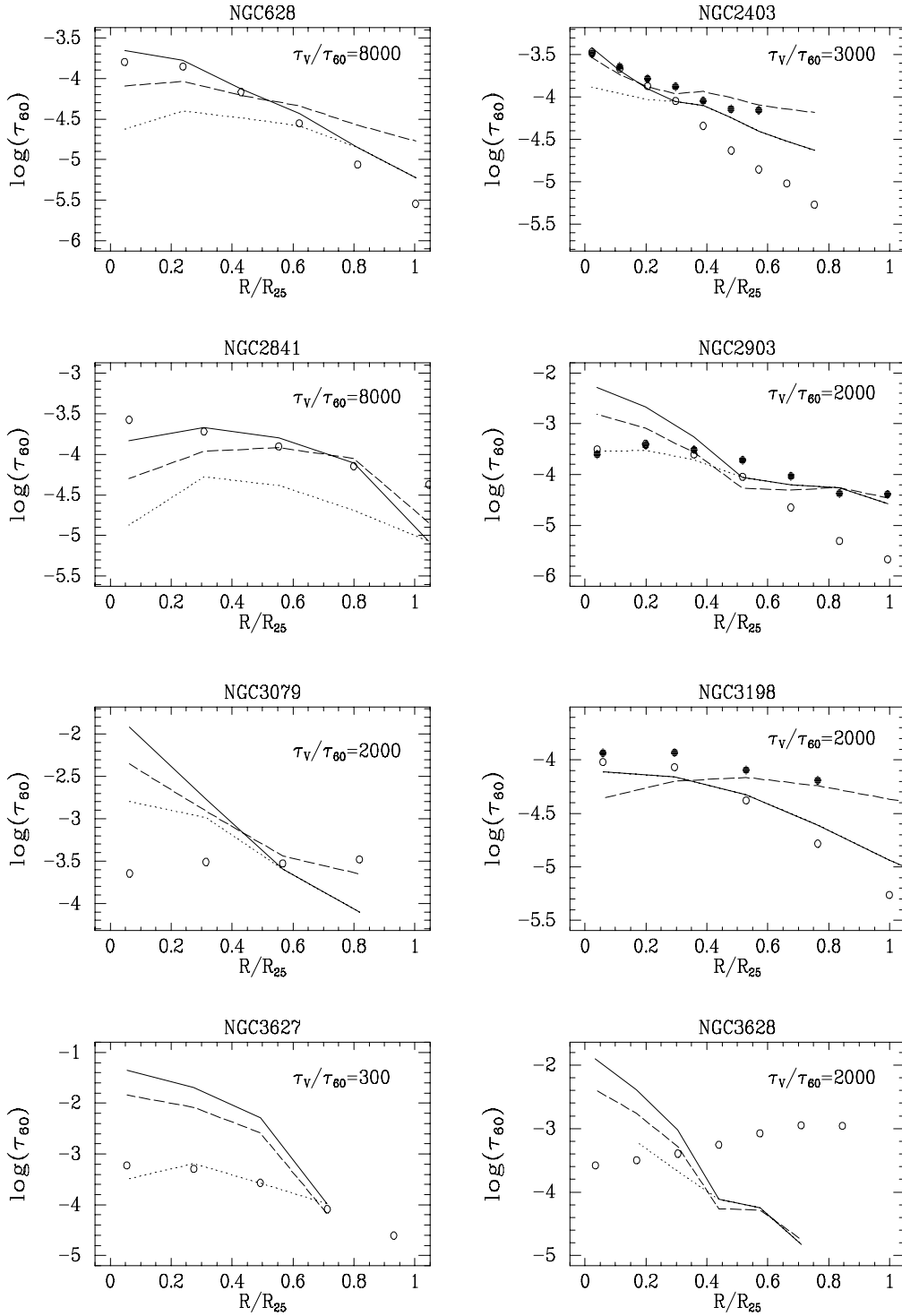


Fig. 5.— The observed τ_{60} radial profiles are compared with that expected from Eq. 5 for the total and atomic hydrogen gas surface densities separately. Open circles are the observed values, whereas the the filled circles (for 13 galaxies) are the estimated τ_{60} values for the big grains alone which make up almost the total dust mass column density. The assumed value of τ_V/τ_{60} is indicated for each galaxy. The last panel explains the meaning of the different lines. See Sec. 4.1 for details.

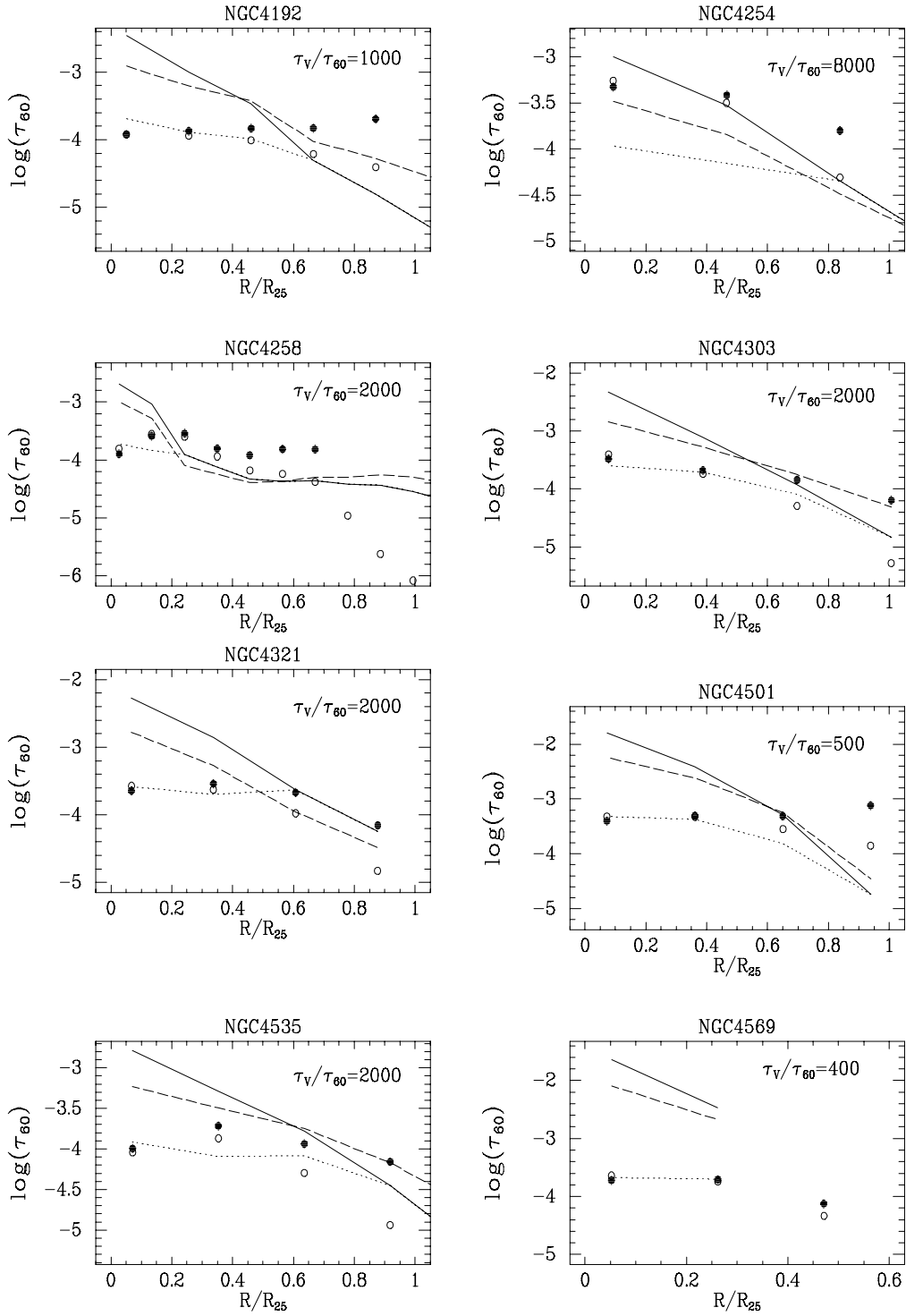


Fig. 5.— Continued.

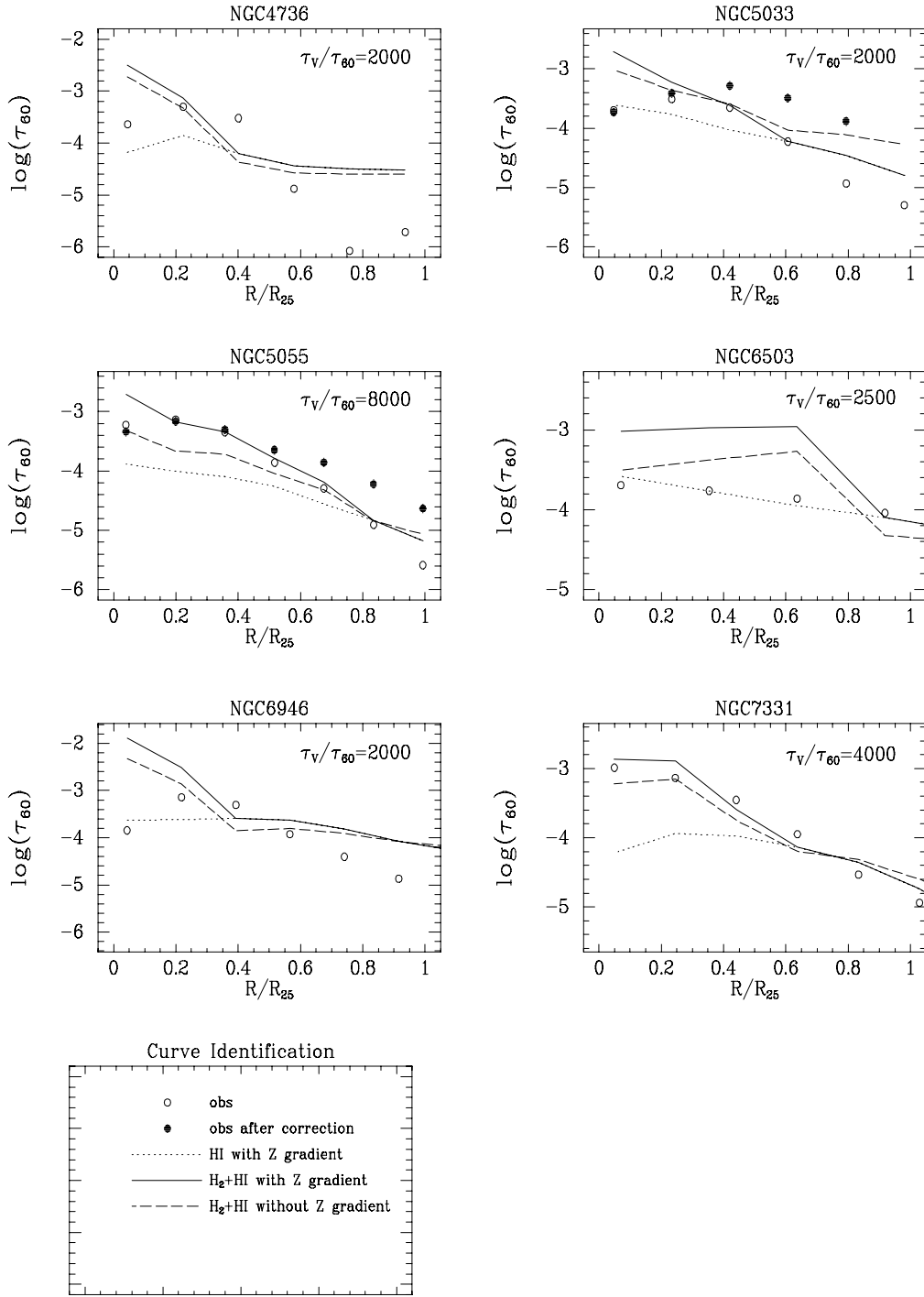


Fig. 5.— Continued.

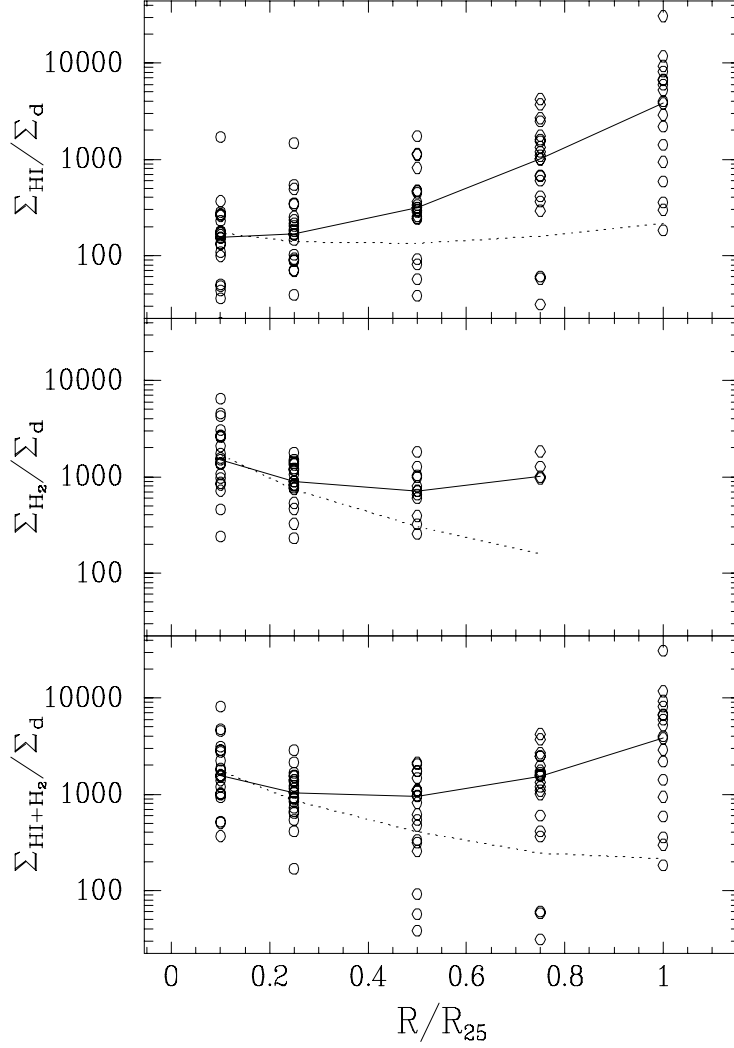


Fig. 6.— Observed values of the gas-to-dust mass surface density ratios in the program galaxies are plotted at distances 10, 25, 50, 75 and 100% of the optical disk radius. At each radius there is one open circle for each galaxy. The solid line passes through the median of the distribution. Dust masses are corrected for the contaminating effects of VSGs and PAHs and the resulting radial profiles are denoted by the dotted lines. Individual atomic and molecular gas masses in the first two panels add up to give the total gas-to-dust ratio of panel 3.

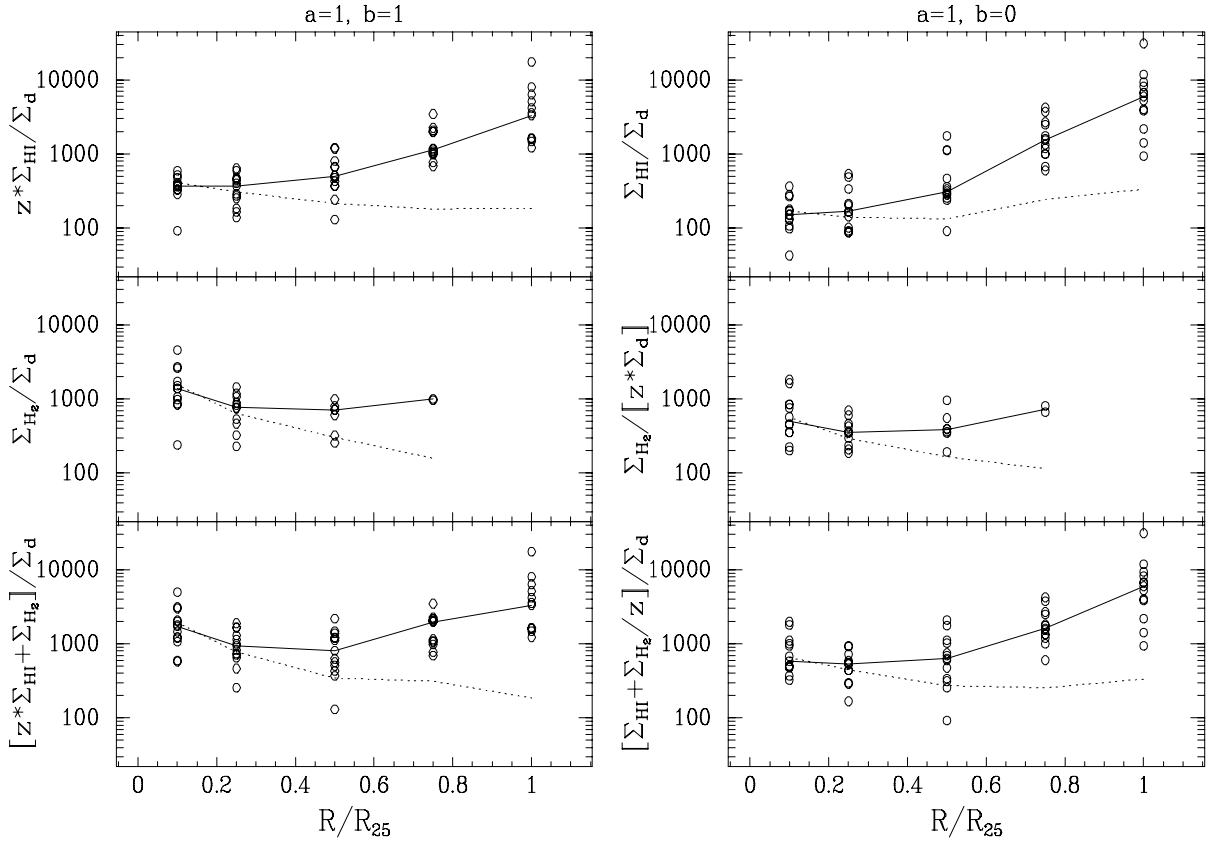


Fig. 7.— The role of metallicity (z) in producing the radial gradients in the gas-to-dust ratio is investigated in this figure. The CO intensity to H_2 mass conversion factor is assumed to depend inversely on z ($a = 1$) in all the plots. The dust fraction is assumed to be proportional to z ($b = 1$) in the left three panels. Other details are similar to that in Fig. 6. The corrected profile is nearly horizontal in the last panel, implying that the dust fraction is independent of z , but the CO intensity to H_2 mass conversion factor indeed depends inversely on z .

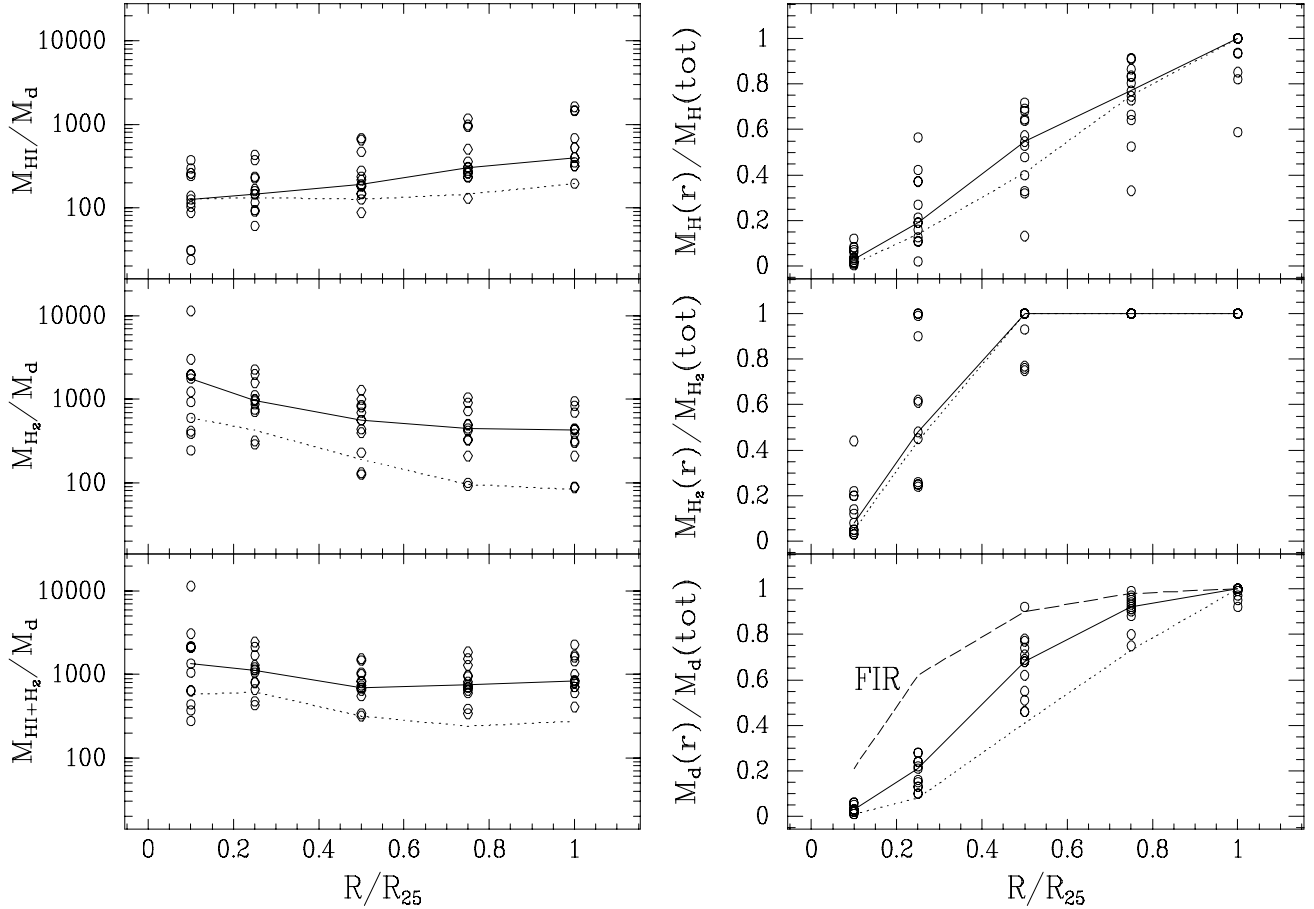


Fig. 8.— The cumulative gas-to-dust mass ratios are plotted as a function of radial distance from the center in the left 3 panels. The solid line and open circles have the same meaning as in Fig. 6. The dotted line here takes into account the correction to the molecular hydrogen mass in addition to the dust mass. Note that the corrected global gas-to-dust ratio is 275, which is within a factor of 2 of the local galactic value, in spite of the bright central regions having values close to 600. This trend of corrected global values being controlled by the gas and dust in the outer disk can be understood from the plots in the right panels. The cumulative fractions of total gas, molecular gas and dust, to the global masses in the respective components are plotted in the three panels. The corrected values are denoted by the dotted line where as the circles and solid lines denote the values for individual galaxies and their medians before corrections. The dashed line in the bottom most panel denotes the cumulative FIR luminosity, 90% of which originates within half the disk radius. Note that the correction increases the mass fraction outside half the disk radius from 30% to 60% for the dust and 45% to 60% for the gas.